

Article ID: 1000-9116(2001)02-0117-12

Three dimensional shear wave velocity structure of crust and upper mantle in South China Sea and its adjacent regions by surface waveform inversion^{*}

CAO Xiao-lin¹⁾ (曹小林) ZHU Jie-shou²⁾ (朱介寿) ZHAO Lian-feng²⁾ (赵连锋)
CAO Jia-min²⁾ (曹家敏) HONG Xue-hai²⁾ (洪学海)

1) School of Computer Science, National University of Defense Technology, Changsha 410073, China

2) Chengdu University of Technology, Chengdu 610059, China

Abstract

We assembled approximately 328 seismic records. The data set was from 4 digitally recording long-period and broadband stations of CDSN. We carried out the inversion based on the partitioned waveform inversion (PWI). It partitions the large-scale optimization problem into a number of independent small-scale problems. We adopted surface waveform inversion with an equal block ($2^{\circ} \times 2^{\circ}$) discretization in order to acquire the images of shear velocity structure at different depths (from surface to 430 km) in the crust and upper-mantle. The resolution of all these anomalies has been established with "check-board" resolution tests. These results show significant difference in velocity, lithosphere and asthenosphere structure between South China Sea and its adjacent regions.

Key words: South China Sea; surface waveform; partitioned waveform inversion; three dimension; shear wave velocity structure

CLC number: P315.2 **Document code:** A

Introduction

Historically, surface waves provided much of our understanding of the lateral heterogeneity in the crust and the upper mantle, especially in oceans or desert areas. Traditional method utilizes the great circle theorem for surface waves. It assumed that surface wave propagates along the great circle connecting epicenter with station. Firstly, traditional surface wave analysis was carried out by using multi-frequency-filter dispersion analysis to acquire the group or phase velocity dispersion curve, which can be used to determine the interior earth velocity structure. These suffer from several drawbacks: ①The great circle theorem is accepted if the lateral heterogeneity is smooth on a scale of a wavelength of the surface wave under consideration. In practice, this condition may not be satisfied (Snieder, 1986). ②It omits multi-pathing and polarization. In some cases an appreciable fraction of the surface wave energy propagates over non-great circle paths. Fur-

^{*} Received date: 1999-12-21; revised and accepted date: 2000-09-11.

Foundation item: State Natural Scientific Foundation (49734150) and National High Performance Computation Foundation.

本文英文审校: 李兴才

thermore, different mode coupling is neglected (Snieder, 1988; Marquering, Snieder, 1996). ③ It is hard to get accurately dispersion curve using multi-frequency-filter analysis. ④ It only analyzes dispersion data without utilizing amplitude information, higher mode surface and scattered surface wave information (Yomogida, Aki, 1987).

In order to solve these problems mentioned above, a complete three-dimensional surface waveform inversion must be carried out. This inversion should take care of the following effects (Snieder, Romanowicz, 1988): ① The inhomogeneities should be located at their correct horizontal position. ② The depth distribution of the heterogeneity should be determined. ③ The different inhomogeneities density, pressure wave velocity and shear wave velocity can be inverted simultaneously. It is clear that a complete three-dimensional heterogeneity reconstruction is hard to realize with a finite set of band-limited and uneven distributing epicenters and stations. Furthermore, the computation of inversion requires prohibitive CPU times. With present data sets there are three realistic approaches: ① Spherical harmonics inversion (Woodhouse, Dziewonski, 1984); ② One can parameterize the depth dependence and the different contributions of density, pressure wave velocity and shear wave velocity in a finite set of basis functions. This may reduce the freedom of the heterogeneous body (Snieder, Nolet, 1987); ③ This allows a two-step inversion of surface wave data. In the first step the scattering is used to find the phase velocity perturbation as function of latitude and longitude. Once these local phase velocities are computed, a standard linear inversion can be used to determine the depth dependence of the heterogeneous body (Snieder, Romanowicz, 1988). In fact, it get firstly the horizontal position of heterogeneous body, then the vertical position so as to acquire the three dimensional position. In recent years, Nolet (1990) presents a new method for nonlinear waveform inversion, partitioned waveform inversion (PWI). Shear wave velocity variations in the upper mantle beneath central Europe were studied by using PWI method (Zielhuis, Nolet, 1994). The resulting 3-D model can accurately predict the real velocity structure. It indicates an optimum resolution of better than 200 km in the Hellenic collision zone with the highest density of wave paths. It also has been applied to study upper mantle shear velocity beneath eastern Australian. Its results can be used to resolve anomalies over 250 km horizontally and 50 km vertically (Zielhuis, Van der Hilst, 1996).

Although PWI method faces up some problems like traditional dispersion, for example it still utilizes the great circle theorem omitting multipathing and polarization. It can utilize not only the phase or group velocity but also the fundamental and higher mode surface waveform and scattered surface waveforms. It is the key that waveform data are directly inverted for seismic velocity so that it shows a good match between the corresponding synthetic seismograms obtained after PWI inversion and the real seismograms, which is very useful to future complete three-dimensional inversion. So we assembled a lot of seismic records and carried out the inversion studying three dimensional shear wave velocity structure of the crust and the upper mantle in South China Sea and its adjacent regions based on the partitioned waveform inversion. The images of shear velocity at different depths in the crust and the upper-mantle show the significant difference of velocity and lithosphere and asthenosphere structure between the blocks of South China Sea and its adjacent regions. Furthermore, in order to avoid the inversion ending up at a local minimum, we use a non-linear optimization search method (simulated annealing algorithm) instead of the conjugate gradient technique.

1 Surface waveform inversion theory

PWI method assumes there is a well-defined region that influences a particular seismic time

series, and firstly the influences of the remaining Earth upon this particular datum can be ignored (Nolet, 1990). It partitions surface waveform inversion for 3-D earth model into two steps. The first step determines path-average velocity between source and receiver by waveform fit using a nonlinear optimization search method; then a 3-D model is produced through assembling all path-average velocities in the second linear inversion step (Zielhuis, Nolet, 1994).

In this text we put forth the following method: the first step determines path-average velocity between source and receiver by one-dimensional surface wave waveform inversion using simulated annealing algorithm. With the use of these linear constraints equation acquired by path-average velocities, a 3-D model is produced in the second linear inversion step by solving equation with LSQR algorithm. Furthermore the synthetic surface waveform is calculated based on the 3D velocity model of shear wave, and then the comparison between the waveform computed and observed is made to check whether the model is correct (ZHU, *et al*, 1997). It costs mainly a large number of CPU times in the first step. Because simulated annealing algorithm is very effective and highly paralleled in finding path average models that predict optimal waveform fitting to observed seismograms. We can calculate an average model of different paths on every node. These make surface waveform inversion computations feasible.

1.1 Calculating synthetic surface waveform

Based on great circle approximation, the far-field response of a laterally homogeneous elastic Earth to a point force can be written (Sneider, Nolet, 1987):

$$s_1(\mathbf{r}, \omega) = \sum_v \mathbf{p}^v(\mathbf{r}, \omega) \frac{\exp i [(l_v + 1/2)\ddot{A} + \delta/4]}{(\sin \ddot{A})^{1/2}} [\mathbf{p}^v(\mathbf{r}_s, \omega) \cdot \mathbf{f}] \quad (1)$$

where D is epicentral distance (radian); \mathbf{r}_s , the vector of $(z_s, \mathbf{q}, \mathbf{f})$, is the source position; \mathbf{r} , the vector of $(z, \mathbf{q}, \mathbf{f})$, is the receiver position; z is the depth; \mathbf{q} is longitude; \mathbf{f} is latitude; \mathbf{f} is a point force; ω is frequency; \mathbf{p}^v is the polarization vector of v -mode surface wave, l_v is related to the horizontal wavenumber of the v -mode surface-wave and $\mathbf{p}^v \cdot \mathbf{f} = p_i^v \times f_i$. Based on above expressions, it is easy to acquire the response to an excitation by a moment tensor

$$s_2(\mathbf{r}, \omega) = \sum_v \mathbf{p}^v(\mathbf{r}, \omega) \frac{\exp i [(l_v + 1/2)\ddot{A} + \delta/4]}{(\sin \ddot{A})^{1/2}} [\mathbf{E}^v(\mathbf{r}_s, \omega) : \mathbf{M}] \quad (2)$$

\mathbf{E}^v is the excitation tensor, \mathbf{M} is the moment tensor, $\mathbf{E} : \mathbf{M} = E_{ij}^v \times M_{ji}$.

We use Thomson-Haskell technique (Schwab, Knopoff, 1972; Panza, 1985) for calculating eigenvalues, eigenfunctions of every mode. With normalization and the minimum layer of thickness, they used a modification of the optimized layer matrix formulation to obtain high-speed algorithm at high frequency without loss of precision. Based on the multi-mode summation algorithm described above, we can synthesize theoretical seismograms in time domain by the Fourier transforming equation (1) or (2).

1.2 Path-average velocity

We firstly assume that perturbations in the Rayleigh surface waveform are only caused by variations in the shear wave velocity $\mathbf{b}(z)$. Pressure velocity $\mathbf{a}(z)$ and density $\mathbf{r}(z)$ are transformed by $\mathbf{b}(z)$ through empirical equation. We must get N_z layer velocity before calculating synthetic surface waveform based on the multi-mode summation algorithm. The path-average velocity is given by $\overline{\mathbf{b}_i^j}(z)$ as following:

$$\overline{\mathbf{b}_i^j(z)} = \mathbf{b}_i^j(z) + \mathbf{db}_i^j(z) \quad i = 1, 2, \dots, N_z \quad (3)$$

where $\mathbf{b}_i^j(z)$ is initial velocity model of the j -th path and $\mathbf{db}_i^j(z)$ is the corresponding velocity perturbation. The multi-layer velocity $h_n(z)$ ($n=1, 2, 3, \dots, N_z$) required for the forward computation is obtained from the expansion of basis functions of $h_m(z)$ at M depths (Du, Panza, 1999). We model the shear wave velocity with a total of 41 depth functions (every 5 km in the depth range 0~100 km, every 10 km in the depth range 100~190 km, every 20 km in the depth range 190~430 km). The study on synthetic and real data shows that it is theoretically possible to determine Moho-depth with an accuracy of less than a kilometer if the frequency range extends to 0.12 Hz (Das, Nolet, 1995). We assembled surface waveform ranging from 10 s to 200 s, so it is possible to obtain good waveform fitting based on the velocity structure. After getting N_z layers $\overline{\mathbf{b}_i^j(z)}$, we can easily compute theoretical seismograms $s(\mathbf{r}, t, \mathbf{db})$ using multi-mode summation algorithm.

Retrieving path-average velocity was transformed into a problem of getting a minimum of object function (Zielhuis, Nolet, 1994). However, as the waveform is a non-linear function of the parameters and sometimes the non-linearity is strong, and the conjugate gradient method or gradient method is not only pertinent to starting velocity model but also is easily trapped in local minimum. Therefore simulated annealing may be applied to such global optimization problems and it does not depend on the initial model. Simulated annealing algorithm bears analogy to nature system and robust in nature. Simulated annealing usually models such a physical process in which a solid in a "heat bath" is warmed by increasing the temperature. This is followed by the slow cooling until the global minimum energy state is reached where a crystal is formed by a proper cooling schedule controls and using Metropolis principle (MA, *et al*, 1997).

In order to invert robustly, we define two object functions taking account of simulated annealing characteristic. To compare the data and synthetics, we define object function as the negative of the "normalized cross correlation" function given by the following equation (4). It is not sensitive to absolute amplitudes of the synthetic and the observed data (HelMBERGER, Engen, 1980).

$$f(\mathbf{db}^j) = 1 - \frac{\int_0^T d_j(t) s_j(\mathbf{r}, t, \mathbf{db}^j) dt}{\left(\int_0^T d_j^2(t) dt \int_0^T s_j^2(\mathbf{r}, t, \mathbf{db}^j) dt \right)^{1/2}} \quad (4)$$

where $d_j(t)$ is observed waveform of the j -th path, $s_j(\mathbf{r}, t, \mathbf{db}^j)$ is the corresponding synthetic surface waveform, T is the length of time series.

In order to study fine velocity structure, we consider not only the correlation but also amplitude difference between the synthetic and the observed data. An alternative and sometimes more useful measure of the object function can be defined by the following equation:

$$f(\mathbf{db}^j) = \frac{\int_0^T |d_j(t) - s_j(\mathbf{r}, t, \mathbf{db}^j)| dt}{\left(\int_0^T d_j(t) dt \right)^{1/2}} \quad (5)$$

In real data processing, we first take into account cross correlation given by equation (4). The misfit function given by equation (5) is only used under the condition that waveforms of the synthetics match well with the observed data. Because simulated annealing algorithm needs heavy

computation, we designed highly paralleled algorithm. These make surface waveform inversion computations feasible on systems as small as a Dawn-1000 parallel computer.

1.3 3-D Earth interior velocity model

After getting $db^j(z)$, it is easy to obtain path-average velocity model $\overline{b^j(z)}$. Quantitative analysis of the result of waveform inversion for one seismic waveform may reach several hundred kilometer in resolution (Gomberg, Masters, 1988). Sometimes the path average themselves may be useful as model, and we may find the average model along one path that is the least complicated model in some sense (Nolet, 1990). In order to obtain 3-D model, the individual source-receiver data resulting from the nonlinear inversion is combined in a second linear inversion step. Finally a usable set of linear constraints equation is yielded for the heterogeneous Earth model.

$$\frac{1}{\Delta_j} \int_0^a \int_{p_1} \left[\mathbf{b}(z, \mathbf{q}, \mathbf{f}) - \overline{\mathbf{b}^j(z)} \right] dz d\mathbf{A} = \mathbf{e}_j \quad j = 1, 2, \dots, K \quad (6)$$

where D_j is the distance of the great circle, p_j is the great circle, \mathbf{D} is the function of latitude q and longitude \mathbf{f} , a is the largest depth of velocity model, \mathbf{e}_j is an deviation amount from its minimum values and $\mathbf{b}(z, \mathbf{q}, \mathbf{f})$ is 3-D Earth interior velocity model. Its matrix is expressed as:

$$\begin{bmatrix} a_{11} & \cdots & a_{1i} & \cdots & a_{1M} \\ \vdots & & \vdots & & \vdots \\ a_{j1} & \cdots & a_{ji} & \cdots & a_{jM} \\ \vdots & & \vdots & & \vdots \\ a_{K1} & \cdots & a_{Ki} & \cdots & a_{KM} \end{bmatrix} \begin{bmatrix} \mathbf{b}_1 \\ \vdots \\ \mathbf{b}_i \\ \vdots \\ \mathbf{b}_M \end{bmatrix} = \begin{bmatrix} \overline{\mathbf{b}^1} + \mathbf{e}_1 \\ \vdots \\ \overline{\mathbf{b}^j} + \mathbf{e}_j \\ \vdots \\ \overline{\mathbf{b}^K} + \mathbf{e}_K \end{bmatrix} \quad (7)$$

where, a_{ji} is the ratio between the ray length of the j -th raypath in the i -th grid unit and the total length of the j -th great circle; \mathbf{b}_i is the velocity of the i -th grid unit, $i=1, 2, \dots, N_q \times N_f \times N_z$. For example, discretizing South China Sea and its adjacent regions ($90^\circ \sim 140^\circ \text{E}$, $12^\circ \text{S} \sim 32^\circ \text{N}$) in cells of $2^\circ \times 2^\circ$ will lead to $N_q=26$, $N_f=23$. Equation (7) can be resolved by using SVD algorithm (ZHU, 1988) or very large system, iterative algorithm (such as LSQR algorithm) in order to obtain 3-D Earth interior velocity model $\mathbf{b}(z, \mathbf{q}, \mathbf{f})$. Especially LSQR algorithm can solve ill-condition equation rapidly and stably. Adding damp factor easily controls the quality of inversion.

2 Procedure for real data

South China Sea lies in the junction of three plates. Eurasia Plate lies in its north sides, Philippine Sea Plate in the west side and Indian Plate in the east (LIU, 1994). They collided one another, which result in complex geological structure of South China Sea.

We assembled approximately 328 seismic records from 195 earthquakes ($5.0 \leq M_s \leq 7.0$, focal depth shallower than 100 km) occurred in South China Sea and its adjacent regions. The data set was from 4 digitally recording long-period and broadband stations of CDSN between 1986 and 1994. These stations include Enshi (30.27°N , 109.49°E), Kunming (25.12°N , 102.74°E), Qiongzong (19.03°N , 109.84°E), Sheshan (31.10°N , 121.19°E) (Figure 1). These long digital seismograph of these stations records three-component seismic data with sampling rate of 1 sps. We only utilize vertical component of Rayleigh waveform. We adopt the Harvard CMT source solution. We carried out the inversion based on PWI method so as to retrieve three dimensional crust and upper mantle shear wave structure of the region.

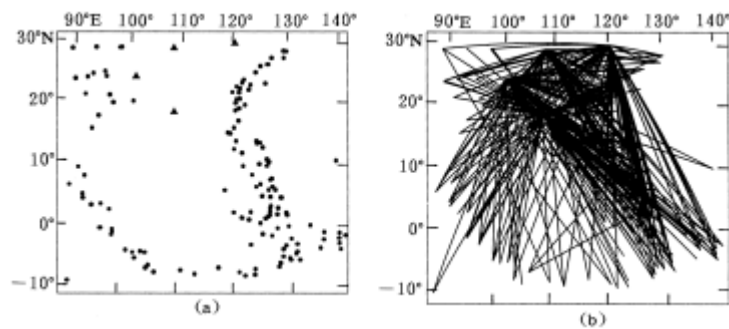


Figure 1 Epicenter and station distribution of South China Sea (a) and distribution of great circle path (b) (Black dot represents epicenter, triangular represents station)

3 Result analysis

3.1 Waveform fitting analysis

To distinguish difference of waveform fitting in the different stages of the inversion process we use the term "individual fitting" for the fitting obtained after non-linear inversion (Figure 2a, 3a); the term "final fitting" refers to the fitting of the waveforms predicted by the 3D model (Figure 2b, 3b). Figure 2a and 2b show the individual fitting and corresponding final fitting of fundamental mode waveform respectively. Figure 3a and 3b show the individual fitting and corresponding final fitting of higher mode fundamental waveform respectively. Generally we obtained good individual fitting (Figure 2a). From Figure 2b we found good agreement between the observed waveforms and the predictions by the final 3D velocity model, but there is a difference in the latter part (such as 1st and 4th seismogram). The cause of the poor fitting in the latter part is as follows: ① In synthetic waveform, we do not take into account attenuation. However the short period of observed data attenuate faster than long period. We normalize the observed data and synthetic waveform, which leads that the amplitude in the latter part of the synthetic waveform is larger than the observed data. ② Small heterogeneity mostly causes the scattered waveforms existing in the latter part of observed waveform. We suspect that this region is characterized by strong heterogeneity, which is difficult to resolve by 3-D resulting model. However these prove that the resulting 3-D model accurately predicts most of the observed fundamental mode surface waveforms, with high resolution.

Figure 3a and 3b shows good fitting of higher mode waveform for most records (see 1st, 4th and 5th seismogram). Some is inferior for fundamental waveform (see 2nd and 3rd seismogram). The inversion of some records (see 1st, 2nd, 3rd, 4th seismogram in Figure 3a and 3b) needs special attention. For example, the waveform is contaminated with other type of waveform, which prohibited an acceptable fit.

3.2 Resolution analysis

Acquiring accurate 3D crust and upper mantle velocity model needs high horizontal resolution and vertical resolution. The horizontal resolution and the vertical resolution are controlled by different factors. The former mainly depends on the distribution and the number of epicenters and stations. The latter depends mostly on the bandwidth of the surface waveform. The path coverage in north part of South China Sea (Figure 1) is reasonably good, which is superior to the south part. There are also wave paths with high density in Sino-Indian block and Philippine islands. So we can deduce that the resolution of north part of South China Sea, Sino-Indian block and Philippine

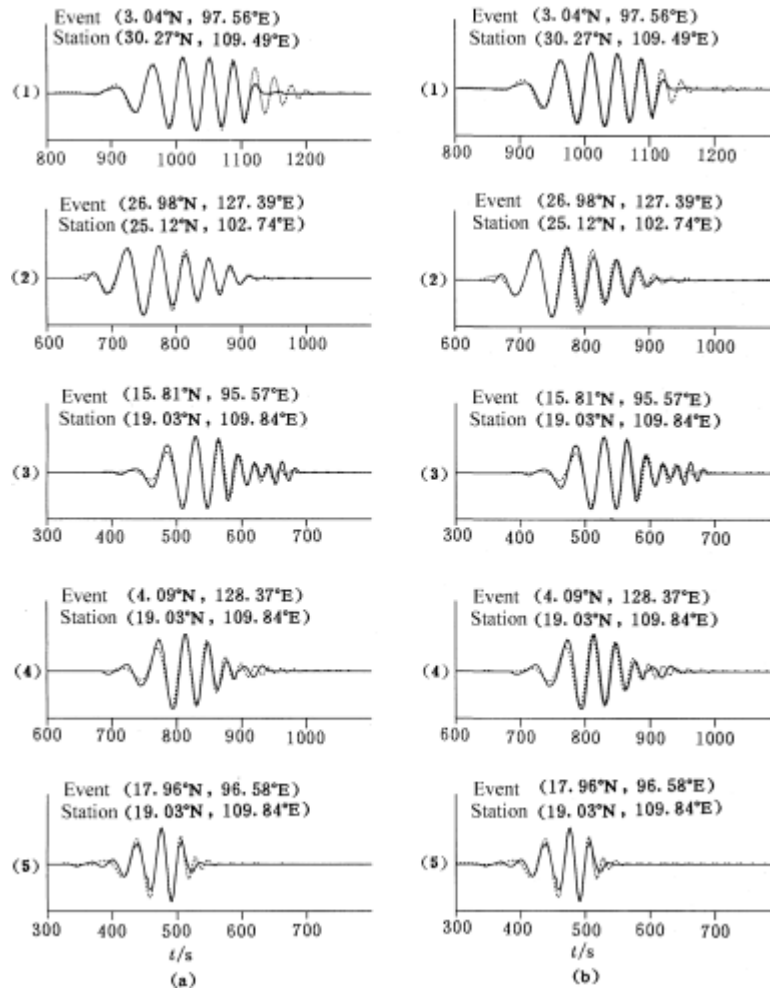


Figure 2 Waveform fitting between observed data (solid line) and synthetic surface waveform (dashed line) of South China Sea regions
 (a) Observations and individual fitting obtained after simulated annealing inversion on the velocity-depth profile; (b) The corresponding observations and predictions by the resulting 3-D model [corresponding to those in (a)]

islands is superior to the other part. In order to investigate the local precision and resolution of the resulting model, we used "checkerboard method" (Ionue, Fukao, 1990). Figure 4 displays there is high resolution in the north part of South China Sea, Sino-Indian block and Philippine islands. In the shallow part of these regions, it can resolve $2^{\circ} \times 2^{\circ}$; in the deep part, it can resolve $4^{\circ} \times 4^{\circ}$. There is low resolution in south part of South China Sea, both in the shallow part and in the deep part can resolve $4^{\circ} \times 4^{\circ}$. Even though the scope of computation is $90^{\circ} \sim 140^{\circ}E$, $10^{\circ}S \sim 25^{\circ}N$, in fact, the scope of resolving effectively is $100^{\circ} \sim 130^{\circ}E$, $0^{\circ} \sim 25^{\circ}N$.

3.3 Velocity distribution characteristics

In order to provide better insight in the 3-D velocity model, we separately show 2 vertical sections of velocity (Figure 5) along latitude $16^{\circ}N$ and along longitude $115^{\circ}E$ and 5 horizontal sections of velocity (at depth of 85 km, 100 km, 120 km, 150 km and 250 km) (Figure 6). More-

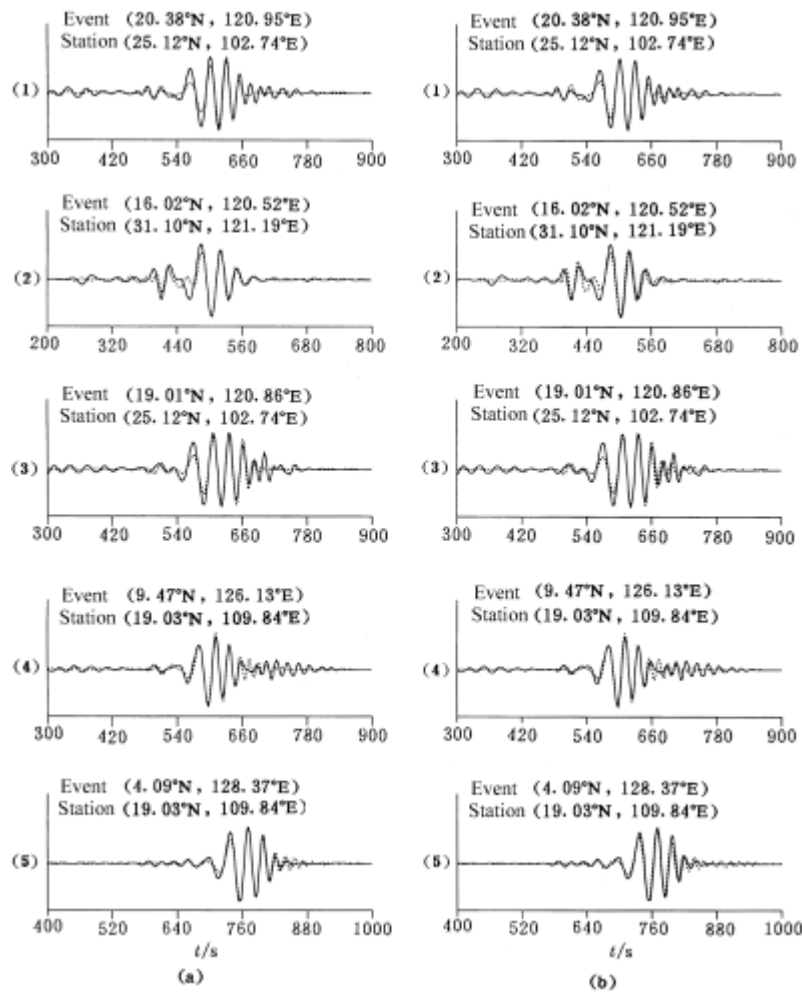


Figure 3 Waveform fitting between observed data (solid line) and synthetic surface waveform (dashed line) of South China Sea regions (Both include higher mode waveform)

(a) Observations and individual fitting obtained after simulated annealing inversion on the velocity-depth profile;
 (b) The corresponding observations and predictions by the resulting 3-D model [corresponding to those in (a)]

over, distribution of asthenospheric boundary depth in South China Sea and its adjacent regions is mapped in Figure 7. From these maps, we can deduce the characteristics of South China Sea and its adjacent regions.

3.3.1 Velocity distribution in the lid of upper mantle

The velocity of 4.40 km/s in the lid of upper mantle in South China Sea basin is relatively low, which is similar to Sino-Indian block in west sides of South China Sea, South China block in northwest sides, Philippine islands in east sides and Pulau Kalimantan in south sides. Among them only in Philippines Sea, the maximum of the velocity is higher than 4.55 km/s, which is shown by the vertical cross-section in Figure 5a (along latitude 16°N) and Figure 5b (along longitude 115°E).

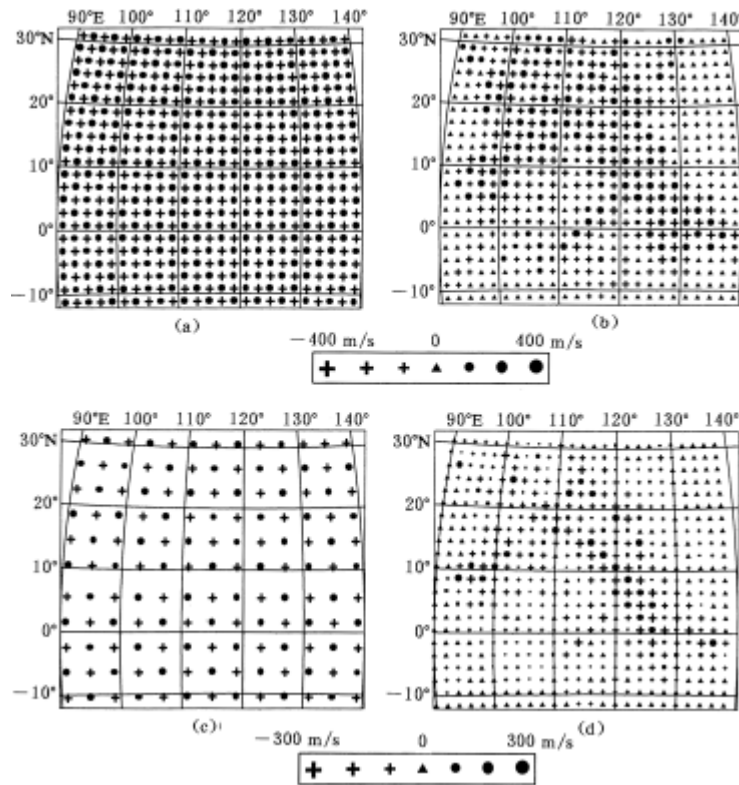


Figure 4 Horizontal resolution test by using "checker-board" method

(a) Forward model at depth of 80 km. An area of anomaly is $2^{\circ} \times 2^{\circ}$. The maximum amplitudes are -400 m/s or 400 m/s. The reference velocity is 4.50 km/s; (b) Inversion result at depth of 80 km; (c) Forward model at depth of 250 km. An area of anomaly is $4^{\circ} \times 4^{\circ}$. The maximum amplitudes are -300 m/s or 300 m/s, the reference velocity is 4.50 km/s; (d) Inversion result at depth of 250 km

3.3.2 Distribute of asthenospheric boundary depth

We define the asthenospheric boundary where its velocities descend and the gradient of velocities is large. The depth of the asthenospheric boundary in South China Sea is shallow, which is about $65 \sim 60$ km. Sino-Indian block in west of South China Sea is about 70 km in depth. The depth of South China block in the northwest is in the range of 70 km to 100 km. Philippine islands is about 65 km in depth. The depth of Taiwan islands in the northeast ranges from 70 km to 85 km. The depth of Philippines Sea block in the east is about 60 km, and the depth of Pulau Kalimantan in the south is about 60 km (Figure 7).

Vertical section of velocity displays more detailed character. In near longitude of 114°E (Figure 5a), the depth of asthenospheric boundary is the shallowest with a depth of 60 km. To the west direction, it becomes gradually deeper up to about 85 km in depth. To the east direction, it first becomes gradually deeper up to about 70 km at the longitude of 120°E firstly and then it becomes gradually shallowest up to about 60 km. In near latitude of 115°E (Figure 5b), the depth of asthenospheric boundary is the shallowest with a depth about 60 km. To the north direction, it becomes gradually deeper up to about 100 km. To the south direction, it becomes deeper up to about 65 km depth firstly and then it becomes gradually shallower up to about 60 km in depth.

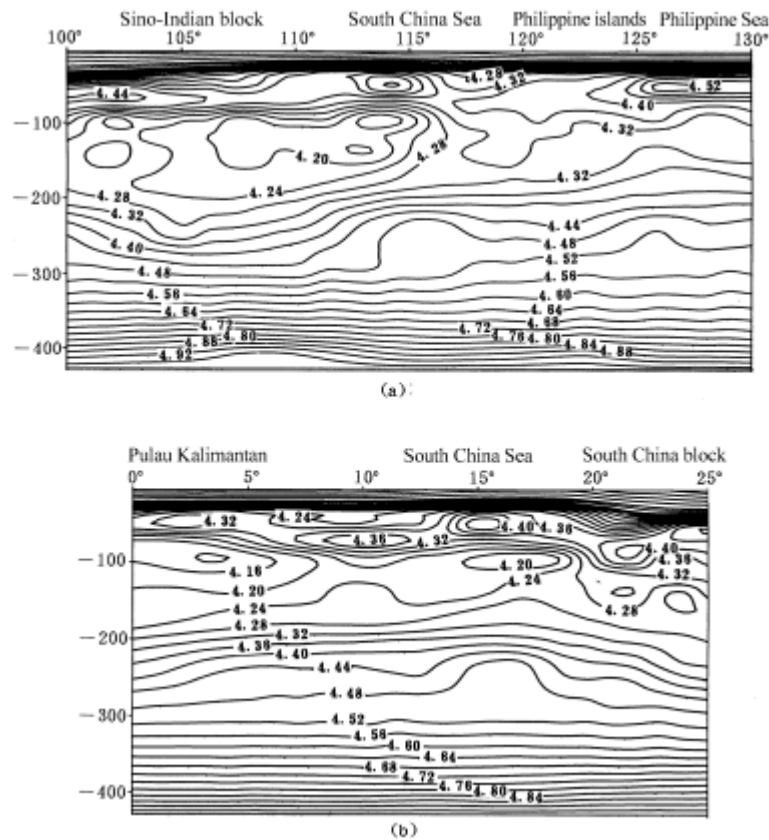


Figure 5 Vertical cross-section of velocity in South China Sea and its adjacent regions along latitude 16°N (a) and along longitude 115°E (b)

3.3.3 Distribution of asthenospheric thickness

We define the lower boundary of asthenosphere with velocity about 4.55 km/s in upper mantle. The lower boundary of asthenosphere change slowly. After getting the depth of upper boundary, it is easy to obtain asthenospheric thickness. Figure 5a displays the depth of asthenospheric thickness in longitude 115°E which is much thick about 250 km. The velocity in asthenosphere ranges from 4.15 km/s to 4.55 km/s. To the west direction, it first becomes thinner and then thicker. In Philippines Sea, the thickness is slightly thin, about 230 km. The minimum velocity is about 430 km/s. Figure 5b displays that the depth of asthenospheric thickness in latitude 16°N is much thick, about 250 km. To the north direction, it becomes thin rapidly. In South China block, it is about 200 km. From 4 horizontal sections of velocity (at depth of 85 km, 100 km, 120 km and 150 km depth) (Figure 6), we can find there exist a quite low-velocity belt up to Pulau Kalimantan. The velocity is about 4.20 km/s.

Viewing from Figure 5 and 6 generally, we can come to the conclusion that asthenospheric thickness in South China Sea basin is very much large about 250 km. The velocity of asthenosphere ranges from 4.15 km/s to 4.55 km/s. In Philippines Sea, the thickness is a bit small about 230 km. The velocity ranges from 4.30 km/s to 4.55 km/s. In Pulau Kalimantan, the thickness is much large about 280 km. The velocity ranges from 4.15 km/s to 4.55 km/s. In South China block, the thickness is relatively small, about 200 km. The velocity ranges from 4.25 km/s to 4.55 km/s.

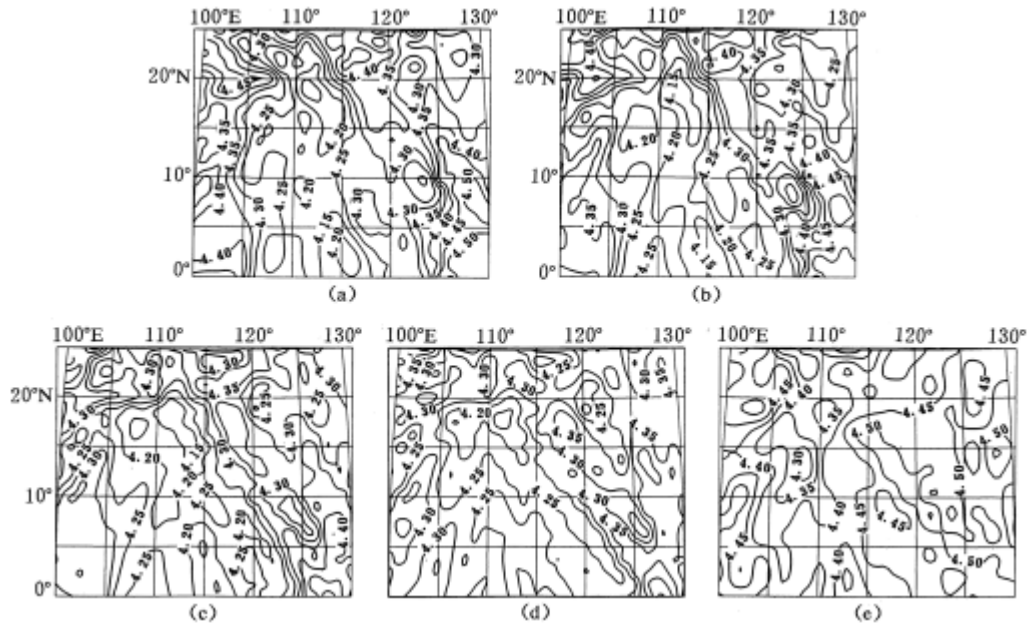


Figure 6 Horizontal cross-section of velocity in South China Sea and its adjacent regions
(a) $h=85$ km; (b) $h=100$ km; (c) $h=120$ km; (d) $h=150$ km; (e) $h=250$ km

In Sino-Indian block, the thickness is about 220 km. The velocity ranges from 4.25 km/s to 4.55 km/s. With the investigation of asthenospheric thickness of global Earth, Anderson (1967) proves that the thickness in ocean regions is much large.

4 Conclusions

We assembled approximately 328 long period seismic records including fundamental and higher mode surface wave. Inversion was carried out studying the three-dimensional shear wave velocity structure of the crust and the upper mantle in South China Sea and its adjacent regions by PWI method. Some conclusions have been recognized:

(1) Simulated annealing algorithm are very effective and highly paralleled in finding path-average velocity models that predict optimal waveform fitting to observed seismograms. Furthermore, it can avoid ending up at a local minimum. PWI method has the potential to yield high-resolution images if enough data are available. In view of the rapid growth of digital broadband data, PWI method therefore holds great promise for the imaging of the crust and the upper mantle structure.

(2) The lid velocity of South China Sea basin is low, about 4.40 km/s. The upper boundary of asthenosphere is low about 65 km. The asthenospheric thickness is very large, about 250 km. The velocity of asthenosphere ranges from 4.15 km/s to 4.55 km/s. The lid velocity of Sino-Indian

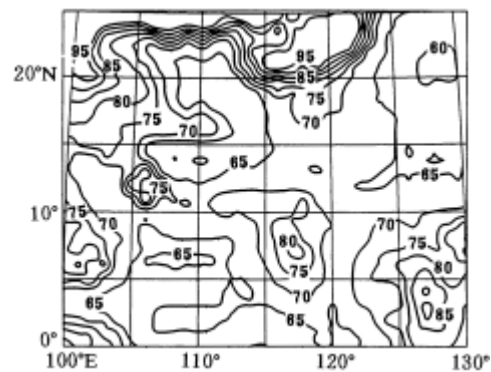


Figure 7 Distribution of asthenospheric boundary depth in South China Sea and its adjacent regions

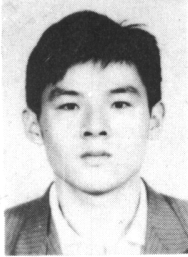
block in west sides of South China Sea is low, about 4.45 km/s. The upper boundary of asthenosphere is relatively shallow, about 70 km. The asthenospheric thickness is about 220 km. The velocity of asthenosphere ranges from 4.25 km/s to 4.55 km/s. The lid velocity of Philippines Sea block is relatively large, about 4.55 km/s. The upper boundary of asthenosphere is shallower, about 60 km. The asthenospheric thickness is about 230 km. The velocity of asthenosphere ranges from 4.30 km/s to 4.55 km/s.

The authors thank CAO Jun-xing, LIANG Chun-tao and PAN Xian-jun for their kind help.

References

- Anderson D L. 1967. Latest information from seismic observations [A]. In: Gaskell T F ed. *The Earth's Mantle* [C]. New York: Academic Press, 355~420.
- Du Zhi-jun, Panza G F. 1999. Amplitude and phase differentiation of synthetic seismograms: A must for waveform inversion at regional scale. [J]. *Geophysics J Intl*, **136**: 83~98.
- Gomberg J S, Masters T G. 1988. Waveform modeling using locked-mode synthetic and differential seismograms: Application to determination of the structure of Mexico [J]. *Geophys J R astr Soc*, **94**: 193~218.
- HelMBERGER D V, Engen G R. 1980. Modeling long-period body waves from shallow earthquakes at regional distances [J]. *Bull Seism Soc Amer*, **70**: 1 699~1 714.
- Inoue H, Fukao Y. 1990. Whole mantle P-wave travel time tomography [J]. *Phys Earth Planet Inter*, **59**: 294~328.
- LIU Guang-ding ed-in-chief. 1994. *Geological and Geophysical Characteristic of China Sea and its Adjacent Regions* [M]. Beijing: Science Press, 1~3 (in Chinese).
- MA Zai-tian, CAO Jing-zhong, WANG Jia-lin, et al. 1997. *Generality of Computational Geophysics* [M]. Shanghai: Tongji University Press, 405~412 (in Chinese).
- Marquering M, Snieder R. 1996. Waveform inversion and the significance of surface-wave mode coupling [J]. *Geophys J Intl*, **124**: 258~278.
- Nolet G. 1990. Partitioned waveform inversion and two-dimensional structure under the Network of Autonomously Recording seismographs [J]. *J Geophys Res*, **95**: 8 499~8 512.
- Panza G F. 1985. Synthetic seismograms: the Rayleigh wave modal summation [J]. *J Geophys Res*, **58**: 125~145.
- Schwab F, Knopoff L. 1972. Fast surface-wave and free mode computation. *Methods in Computational Physics* [M]. New York: Academic Press, 87~180.
- Snieder R. 1986. 3-D linearized scattering of surface waves and a formalism for surface wave holography [J]. *Geophys J R astr Soc*, **84**: 581~605.
- Snieder R. 1988. Large-scale waveform inversions of surface waves for lateral heterogeneity, 2, Application to surface waves in Europe and the Mediterranean [J]. *J Geophys Res*, **93**: 12 067~12 080.
- Snieder R, Nolet G. 1987. Linearized scattering of surface-wave on a spherical earth [J]. *J Geophys Res*, **61**: 55~63.
- Snieder R, Romanowicz B. 1988. A new formalism for the effect of lateral heterogeneity on normal models and surface waves, I, Isotropic perturbations, perturbations of interfaces and gravitational perturbations [J]. *Geophys J R astr Soc*, **92**: 207~221.
- Woodhouse J H, Dziewonski A M. 1984. Mapping the upper mantle: Three-dimensional modelling of Earth structure by inversion of seismic waveforms [J]. *J Geophys Res*, **89**: 5 953~5 986.
- Yomogida K, Aki K. 1987. Amplitude and phase data inversion for phase velocity anomalies in the Pacific Ocean basin [J]. *Geophys J R astr Soc*, **88**: 161~204.
- ZHU Jie-shou. 1988. *Computational Method in Seismology* [M]. Beijing: Seismological Press, 35~47 (in Chinese).
- ZHU Jie-shou, CAO Jia-min, LI Xian-gui, et al. 1997. Three-dimensional initial model of China and adjacent regions [J]. *Acta Geophysica Sinica*, **40**(5): 627~648 (in Chinese).
- Zielhuis A, Nolet G. 1994. Shear-wave velocity variations in the upper mantle beneath Central Europe. [J]. *Geophys J Intl*, **117**: 695~715
- Zielhuis A, Van der Hilst R D. 1996. Upper mantle shear velocity beneath eastern Australian from inversion of waveforms from SKIPPY portable arrays [J]. *Geophys J Intl*, **127**: 1~16.

Contribution to this issue



CAO Xiao-lin (曹小林) Received his PhD from the Speciality of Geophysics, Department of Applied Geophysics, Chengdu University of Technology in 2000. Mainly engaged in the researches on computational mathematics in Computer School of National University of Defense Technology.



DIAO Gui-ling (刁桂苓) Professor of Seismological Bureau of Hebei Province. Graduated from the Chemistry Speciality, Hebei Normal University in 1975. Ever engaged in the researches on the seismological observation and seismicity analysis. Now mainly engaged in the researches on the prediction of earthquake, the relationship among stress field, focal fault and geological tectonic. Member of Chinese Geophysical Society and Chinese Seismological Society.



LI Juan (李娟) Graduated from the Speciality of Geophysics, University of Science and Technology of China in 1997. Received her M.S. from the Center for Analysis and Prediction, China Seismological Bureau in 2000. Now study as a PhD student in Institute of Geophysics of CSB. The research field focus on seismic hazard analysis and geometry fractal. Member of Chinese Geophysical Society.



WANG Shuang-xu (王双绪) Senior Engineer of the Second Crustal Deformation and Monitoring Center, China Seismological Bureau. Graduated from the Speciality of Geodesy, Wuhan Technical University of Surveying and Mapping in 1982. Mainly engaged in the researches on crustal deformation and earthquake analysis and prediction. Member of Chinese Seismological Society, Surveying and Mapping Society of China.